Korean J. Chem. Eng., 33(1), 290-298 (2016)
DOI: 10.1007/s11814-015-0122-y

pISSN: 0256-1115
eISSN: 1975-7220

High surface area polyaniline nanofiber synthesized in compressed CO_2 and its application to a hydrogen sensor

Quoc Minh Pham and Sunwook Kim†

School of Chemical Engineering, University of Ulsan, Ulsan 680-749, Korea
(*Received 17 January 2015 • accepted 8 June 2015*)

Abstract−High surface area polyaniline (HSA PANI) nanofibers were synthesized through oxidative polymerization of aniline in compressed CO_2 using cobalt chloride as an additive. SEM and TEM analyses showed that the HSA PANI nanofibers had a coarse surface of very thin nanofibers. The HSA PANI nanofibers had a fairly uniform diameter range of 70-90 nm with a length of 0.5-1 μm, and showed an electrical conductivity (EC) of 3.46 S/cm. TGA analysis revealed that the HSA PANI nanofibers had more doping substances than did ordinary PANI nanofibers. In the case of the HSA PANI nanofibers, direct measurement of the surface area using gas adsorption method showed high value of 68.4 m^2/g, which was nearly twice that of ordinary PANI nanofibers. The HSA PANI nanofibers were used to fabricate the hydrogen sensor, exhibiting a large increase in resistance upon exposure to hydrogen gas. The hydrogen sensor in this work showed excellent characteristics, such as high sensitivity and short response time. The limit of detection (LOD) and limit of quantification (LOQ) of the hydrogen sensor were very low to show 40 ppm and 133 ppm of hydrogen, respectively.

Keywords: Carbon Dioxide, Polyaniline, Nanofiber, Hydrogen Sensor

INTRODUCTION

Among various conducting polymers, polyaniline (PANI) has been utilized extensively since it has environmental stability, tunable conductivity switching between insulating and semiconducting materials, easy acid/base doping/dedoping, and reversible redox behavior. Recent applications of PANI have been extended further to diverse areas such as electronics, sensors [1-6], wastewater treatment [7-10], and energy storage devices [11,12]. It has been well recognized that the chemical and physical properties of PANI are strongly dependent on the dopants and surface areas of the particles. The high surface area of the fibrous PANI has great advantages for industrial applications, and high surface area (HSA) PANI nanofiber showed greater sensitivities and faster response times than those of its bulk counterparts when used as gas sensors [13,14]. Mi et al. [15,16] also reported that PANI nanofibers exhibited good electrochemical performance with high specific capacitance, which could be attributed to a large effective surface area.

In the oxidative chemical polymerization of aniline, the variation of the synthetic conditions may produce different types of nanostructured PANI [17-20]. For example, the pH of the reacting media greatly affects the morphology and chemical/electrical properties of the product [19,20]. There have been various approaches utilizing chemical and physical methods for the synthesis of PANI nanofibers. Huang et al. [13] prepared PANI nanofibers through interfacial polymerization without the use of a template. We also reported the synthesis of PANI nanofibers through the polymerization of aniline at the interface of compressed CO_2 and an aqueous solution in a high-pressure stirred reactor [21]. It may be said that recent researches for the synthesis of PANI have been focused on the preparation of the HSA PANI nanofibers. The PANI nanofibers with a dendritic structure may be a representative example among the researches relating to HSA PANI. Zhang et al. [22] showed that PANI nanotube dendrites could be synthesized through chemical polymerization utilizing a self-assembly process with naphthalene sulfonic acid derivatives as dopants. Li et al. [23] reported the synthesis of radially aligned PANI dendrites with rectangular hollow interiors using tartaric acid as a dopant. Guo and Zhou [24] prepared dendritic PANI nanofibers by employing acid additives, e.g., H_3PO_4, H_2SO_4 and HNO_3, through electrochemical polymerization. Thanpitcha et al. [25] showed that dendritic PANI nanoparticles were synthesized under acidic conditions in the presence of carboxymethylchitin. In addition to the acid additives, inorganic salts have been used to prepare PANI nanofibers with high surface area. Zhang et al. [26] showed that chrysanthemum flower-shaped PANI nanofibers were prepared by adding inorganic salt. The synthesized PANI nanofibers had a thin diameter (17-23 nm) as well as a high conductivity (~3.7 S/cm) and high crystallinity due to low rate of accretion or elongation of the nanofibers.

Recently, conductive polymers including PANI have been investigated extensively for hydrogen storage [11,27-31] and detection [3,32-34]. Hydrogen has received great attention due to its possible utilization as a clean energy source in the areas of electric generation and automobiles. However, for the safe use of hydrogen, leak detection at very low level is prerequisite and it may be accomplished through the development of highly sensitive hydrogen sensors. Virji et al. [32,33] reported that hydrogen interacted directly with doped PANI nanofibers to induce a conductivity change, which

†To whom correspondence should be addressed.
E-mail: swkim@ulsan.ac.kr

could be useful for the detection of hydrogen gas. The sensitivity of a hydrogen sensor depends on the interaction capacity of hydrogen gas with doping functional group of PANI nanofibers, and it is also affected by the surface area and the electrical conductivity of the materials. Therefore, a hydrogen sensor fabricated using HSA PANI nanofibers may have great advantages in terms of both signal magnitude and response time.

The reaction medium used in this work, carbon dioxide, either in supercritical or subcritical state, provided an excellent means for producing various morphologies of nanomaterials. The unique physical properties of supercritical fluids made it possible to expand their application areas from traditional extraction processes to various fields such as chemical synthesis and the preparation of nanostructured materials [35-39]. Compared to supercritical carbon dioxide, the properties of subcritical compressed CO_2 are less adjustable. However, the actual solvating powers of subcritical compressed CO_2 may be strong while maintaining environmental benefits as a possible alternative to conventional solvents.

In this work, PANI nanofibers were prepared through the polymerization of aniline in compressed CO_2 by adding cobalt chloride as an additive. The produced nanofibers had solid cores and dendritic structures with high surface areas, and those were utilized for the fabrication of a hydrogen sensor. The hydrogen gas was detected through the measurement of resistance change.

EXPERIMENTAL

1. Materials

Aniline, cobalt (II) chloride, and ammonium peroxydisulfate ($(NH_4)_2S_2O_8$) (APS) were purchased from Merck. High purity carbon dioxide (99.999%) was provided by Korea Gas Tech (KGT) Company. All the chemicals were reagent grade and used as received without any further purification.

2. Experimental Equipment

The reactions in compressed CO_2 were performed using a high-pressure stirred reactor (R-201, Reaction Engineering, Inc.) equipped with magnetic drive as described in the previous investigation [21]. Electrical conductivity (EC) measurements were performed on compressed powder pellets with a conventional four-point probe technique at 20 °C using a Keithley 237 high-voltage source measuring unit. Fourier-transform infrared (FT-IR) spectra were obtained with a resolution of 1 cm^{-1} in the range of 400-4,000 cm^{-1} using a Nicolet 380 FT-IR spectrometer. Thermogravimetric analysis (TGA) was performed with a TA (TGA-Q50) instrument at a heating rate of 10 °C/min. The morphologies of the prepared materials were characterized using SEM, EDS (JSM-6300). And the TEM images were taken using Hitachi H-7500 at an accelerating voltage of 200 kV. The TEM samples were prepared by depositing solids onto a carbon copper grid using dispersed solution of PANI in ethanol. X-ray diffraction (XRD) patterns were obtained with a Rigaku D/MAX-2200 powder X-ray diffractometer using a Cu Ka α radiation source (λ=0.1543 nm). The X-ray tube was operated at 35 kV, 20 mA, and the 2θ angle was scanned from 10-100° (stepwise 0.02°) at a speed of 2°/min. The surface areas of the samples were measured using a gas adsorption method (ASAP 2020, Micromeritics). Prior to the measurement, the samples were degassed under vacuum at 200 °C for 6-12 hrs.

3. Preparation of PANI Nanofibers

The PANI nanofibers were synthesized through the chemical oxidative polymerization of aniline in an acidic environment with APS as an oxidant [13], and the polymerization occurred at the interface of CO_2 and the aqueous solution in a high-pressure stirred reactor [21]. To synthesize HSA PANI nanofibers in compressed CO_2, the previous procedure [21] was modified by adding cobalt chloride into aqueous solution. The molar ratio of aniline and cobalt chloride was varied from 6 : 1 to 1 : 1 and 1 : 6. In a typical experiment with a 1 : 1 molar ratio of aniline and cobalt chloride, $CoCl_2$ (13.64 g) was dissolved in 150 mL hydrochloric acid (1 M) aqueous solution. Then, the aqueous acidic solution and 6 mL aniline were placed in a 500 mL high pressure reactor. While maintaining temperature of the reactor at 10 °C, CO_2 was compressed into the reactor up to 5.53 MPa using a high-pressure syringe pump, and the reactor was stirred continuously at 450 rpm for 1 hr. The injector containing 6 g of initiator (APS) and 14 mL water was compressed with CO_2 up to 13.9 MPa. By opening the valve between the reactor and injector, the initiator mixture could be introduced into a high-pressure reactor. After initiator injection was finished, CO_2 was compressed into the reactor until the pressure reached 13.9 MPa. Aniline dissolved in compressed liquid CO_2 was polymerized at the interface of CO_2 and the aqueous solution. After 5 hrs of reaction, CO_2 was vented and the remaining solution was centrifuged to recover particles. The products were washed several times with deionized water and ethanol, and were dried in a vacuum oven at 40 °C for 12 hrs.

4. Hydrogen Sensor Test

The hydrogen sensor was designed and fabricated using HSA PANI nanofibers so as to operate as a resistivity element. The sensor was composed of two physical components: the sensitive PANI nanofiber layer and the transducer. Two aluminum (Al) electrodes were patterned on a SiO_2/Si substrate with a conventional lithography technique, and the distance between the electrodes was 4 mm. The HSA PANI nanofibers were then deposited onto a SiO_2/Si substrate through the spin coating of nanofibers at a speed of 500 rpm for 50 seconds. The prepared PANI film was dried in a nitrogen atmosphere at 25 °C. The sensor was mounted inside the enclosed cell where the concentration of H_2 in N_2 gas could be adjusted by using a computerized mass flow controller system (MFC MPR-2000 Nanohitec Company). The gas mixture was delivered into the cell at a constant flow rate of 10 sccm, and the exposure time for each pulse of H_2 gas was fixed. For a periodic test of the device, the cell was purged with compressed air between each pulse of hydrogen gas in order to restore the sensor surface to the original condition. The real-time resistance changes of the sensor were recorded every 0.1 seconds with a Keithley 4200-SCS by applying a bias of 4 V between two electrodes.

RESULTS AND DISCUSSION

1. Morphology of PANI Nanofibers

The SEM and TEM images of the PANI nanofiber samples are shown in Figs. 1 and 2, respectively. In this work, the PANI nanofibers produced without an additive were called ordinary PANI nano-

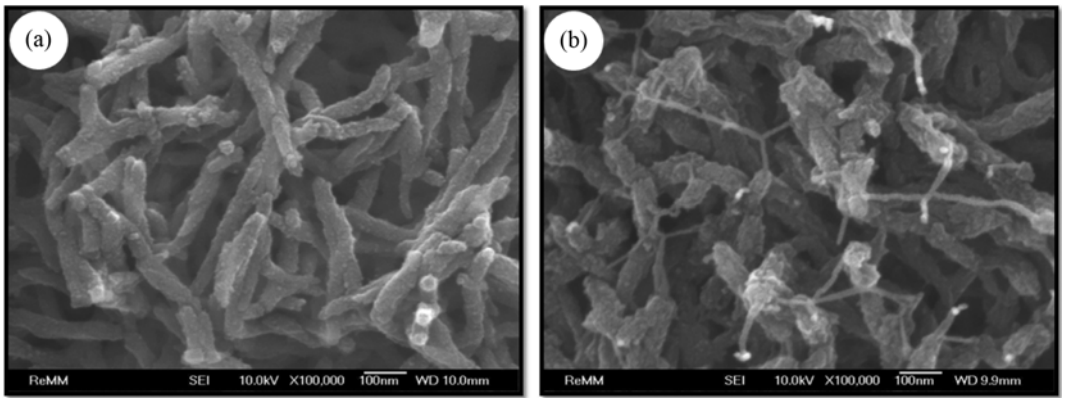

Fig. 1. SEM images of (a) ordinary PANI nanofibers and (b) HSA PANI nanofibers synthesized in compressed CO_2.

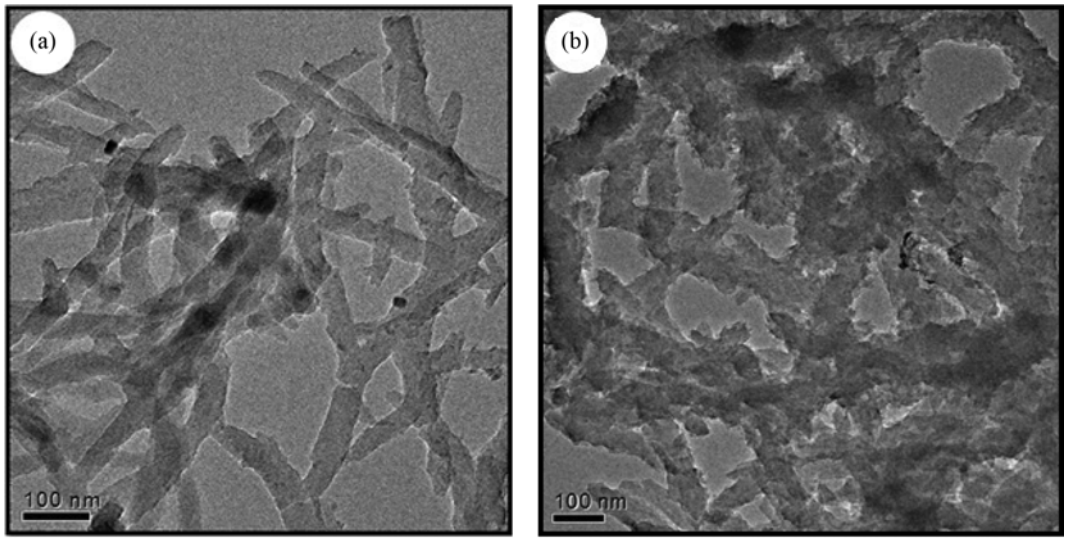

Fig. 2. TEM images of (a) ordinary PANI nanofibers and (b) HSA PANI nanofibers synthesized in compressed CO_2.

fibers to distinguish from the high surface area PANI (HSA PANI) nanofibers. As shown in Figs. 1(a) and 1(b), ordinary PANI nanofibers and HSA PANI nanofibers exhibited similar fibrous forms, but had different dimensions and surface characteristics. The HSA PANI nanofibers revealed a coarse surface and very thin PANI nanofibers (<10 nm diameter) connected between the nanofiber backbones. Moreover, the HSA PANI nanofibers had larger diameters than those of the ordinary PANI nanofibers. The diameters of the HSA PANI nanofibers were 70-90 nm, while those of the ordinary PANI nanofibers were 30-70 nm. Although the diameters of the two PANI nanofibers were different, the lengths of both PANI nanofibers were within 0.5-1 μm.

The TEM image of the ordinary PANI nanofibers in Fig. 2(a) shows that the nanofibers were not hollow with solid cores. By using cobalt chloride as an additive in the reacting mixture, the dendrites of small PANI fibers grew on the surfaces of PANI backbones to produce the HSA PANI nanofibers as shown in Fig. 2(b). The very thin nanofibers (<10 nm diameter) connecting PANI backbones may be identified at the lower part of Fig. 2(b). Based on the morphologies of the PANI nanofibers, it can be said that the HSA PANI nanofibers have greater surface area than that of ordinary PANI nanofibers. The high surface area of HSA PANI nanofibers could be very promising for practical application due to possible high loading of doping substances.

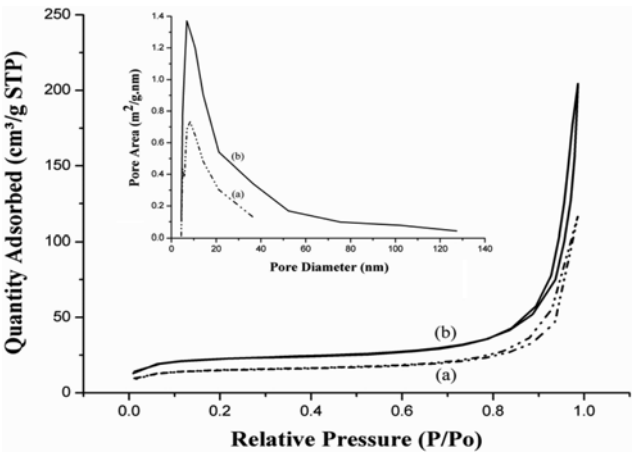

Fig. 3. Nitrogen adsorption-desorption isotherms for (a) ordinary PANI nanofibers and (b) HSA PANI nanofibers.

2. Surface Areas of the Ordinary and HSA PANI Nanofibers

The nitrogen adsorption-desorption isotherms for PANI nanofibers are shown in Fig. 3. The specific surface areas measured according to the BET method for the ordinary and HSA PANI nanofibers were 37.9 and 68.4 m^2/g, respectively. When the relative pressure (P/Po) was below 0.8, the adsorption-desorption isotherms did not show any hysteresis and changed linearly with a very low slope, which was typically observed in nonporous samples. However, at a relatively high relative pressure range (0.8-1.0), the adsorbed amount increased abruptly and the isotherms showed hysteresis. It is believed that the adsorption-desorption behavior at the relative partial pressures of 0.8-1.0 was caused by textural porosity due to the spaces formed by aggregate contacts. The sizes of the textural mesopores were determined by the size, shape, and number of interfacial contacts within the aggregates. We verified the presence of textural porosity by the appearance of a well-defined hysteresis loop in the N_2 adsorption-desorption isotherms in the P/P_o ranging from 0.8 to 1.0. The HSA PANI nanofibers showed a broad pore size distribution compared to that of the ordinary PANI nanofibers, and the pore area of the HSA PANI nanofibers was nearly twice that of the ordinary PANI nanofibers. It is believed that the formation of very thin nanofibers on the surfaces of the HSA PANI nanofibers resulted in large pore areas and a broad pore size distribution.

3. Effect of Cobalt Chloride on the Preparation of HSA PANI Nanofibers.

It has been reported that the polyaniline nanofibers were synthesized through the template-free oxidative chemical polymerization in low pH acidic aqueous media at room temperature [42]. In these conditions, the quasi-linear semi-rigid pernigraniline structure generated at the early stage of polymerization could dictate the formation of the PANI nanofibers in the oxidative chemical polymerization of aniline [40-42]. At the initial stage of chemical oxidative polymerization of aniline, primary PANI nanofibers were formed due to the original structure of the PANI chains [13,43, 44]. The cationic radicals of the aniline and oligomeric intermediates were present near the primarily formed PANI nanofibers, and the nanofibers were able to grow continuously and elongate in one direction [44-47]. Therefore, the principles of the various preparation methods of PANI nanofibers essentially depend on the method of controlling the reaction between the cationic radicals of aniline and the primarily-formed PANI nanofibers. Zhang et al. [48] reported that newly formed PANI nanofibers at the interface were continuously drawn into the aqueous phase. Chiou et al. [44,49] also showed that PANI nanofibers could be prepared through dilute polymerization, and the aniline and oxidant were consumed instantly during the formation of primary nanofibers. In our previous investigation [21], the PANI nanofiber formation was explained by the polymerization of aniline at the CO_2/aqueous solution interface. Aniline has two functional groups with different polarities, and the polar portion of the molecule tends to orient toward the aqueous phase. The nanofibers formed at the CO_2/aqueous interface maintained their fibrous forms and were successfully preserved in the aqueous phase.

In addition to the preparation methods of nanofibers, an interesting observation was obtained by Zhang et al. [26], where the rate of accretion or elongation for the PANI nanofibers was decreased by the presence of inorganic salts. As a result, thinner PANI nanofibers were formed when inorganic salts were used as additives. Based on this observation, it was expected that new forms of PANI nanofibers could be produced through interfacial polymerization by adding inorganic salt in the reacting mixture. Moreover, the impregnation with metal ions may enhance the electrical, magnetic and thermal properties of produced PANI nanofibers. The previous investigation by Gupta et al. [50] showed that cobalt chloride doped polyaniline had greater thermal stability and crystallinity compared to pure polyaniline. Therefore, in this work, cobalt chloride was employed as an additive, and cobalt ions in the aqueous solution played an important role for the formation of small diameter PANI nanofibers during polymerization. As shown in Fig. 4(b), very thin PANI nanofibers (5-10 nm diameters) with lengths of several hundred nanometers were attached to the nanofiber backbones. The HSA PANI nanofibers in Figs. 1-3 were prepared by using an equal molar ratio of aniline and cobalt chloride.

The morphology of the HSA PANI nanofibers was believed to be affected by the formation rates of the nanofiber backbone and the thin nanofibers. If the formation rate of the thin nanofibers was negligible, the resulting product was ordinary PANI nanofibers. Since the formation of thin nanofibers was caused by the addition of cobalt chloride, three different molar ratios of aniline and cobalt chloride, 6 : 1, 1 : 1 and 1 : 6, were employed to investigate the effect of cobalt chloride on the morphologies of prepared PANI nanofibers. When the molar ratio of aniline and cobalt chloride was 6 : 1 (Figs. 4(a) and 4(a')), the products were primarily PANI nanofibers because the formation rate of the nanofiber backbone was greater than that of thin nanofibers. Increasing the relative amount of cobalt chloride from 6 : 1 to 1 : 1, the PANI nanofiber dendrites were formed through the attachment of very thin PANI nanofibers (5-10 nm diameters) onto the PANI backbone surfaces as shown in Figs. 4(b) and 4(b')). Further increasing relative amount of cobalt chloride (1 : 6) caused the predominant formation of thin nanofibers that were interlaced or interpenetrated to form high surface area PANI nanofibers as shown in Figs. 4(c) and 4(c'). Even though the change of morphologies has been explained by the formation rates of the nanofiber backbone and the thin nanofibers, further systematic investigations about reaction rates would be beneficial to elucidate the formation mechanism of HSA PANI nanofibers through interfacial polymerization.

4. Electrical Conductivity (EC) and Thermal Behavior of PANI Nanofibers

The electrical conductivity of PANI nanofibers was measured by using a standard four-point probe method at 20 °C. The electrical conductivity of ordinary PANI nanofibers and the HSA PANI nanofibers showed high values of 4.34 and 3.46 S/cm, respectively. Those values are much greater than the EC of PANI particles. It is well known that the electrical conductivity of PANI depends both on its capacity to transport charge carriers along the polymer backbone and on the movement of carriers between the polymer chains [51]. Since the PANI nanofibers were highly crystalline and had branchless long chains, the PANI nanofibers showed more favorable transport charge carrier characteristics compared to those of the PANI particles. As mentioned previously, the EC of the HSA

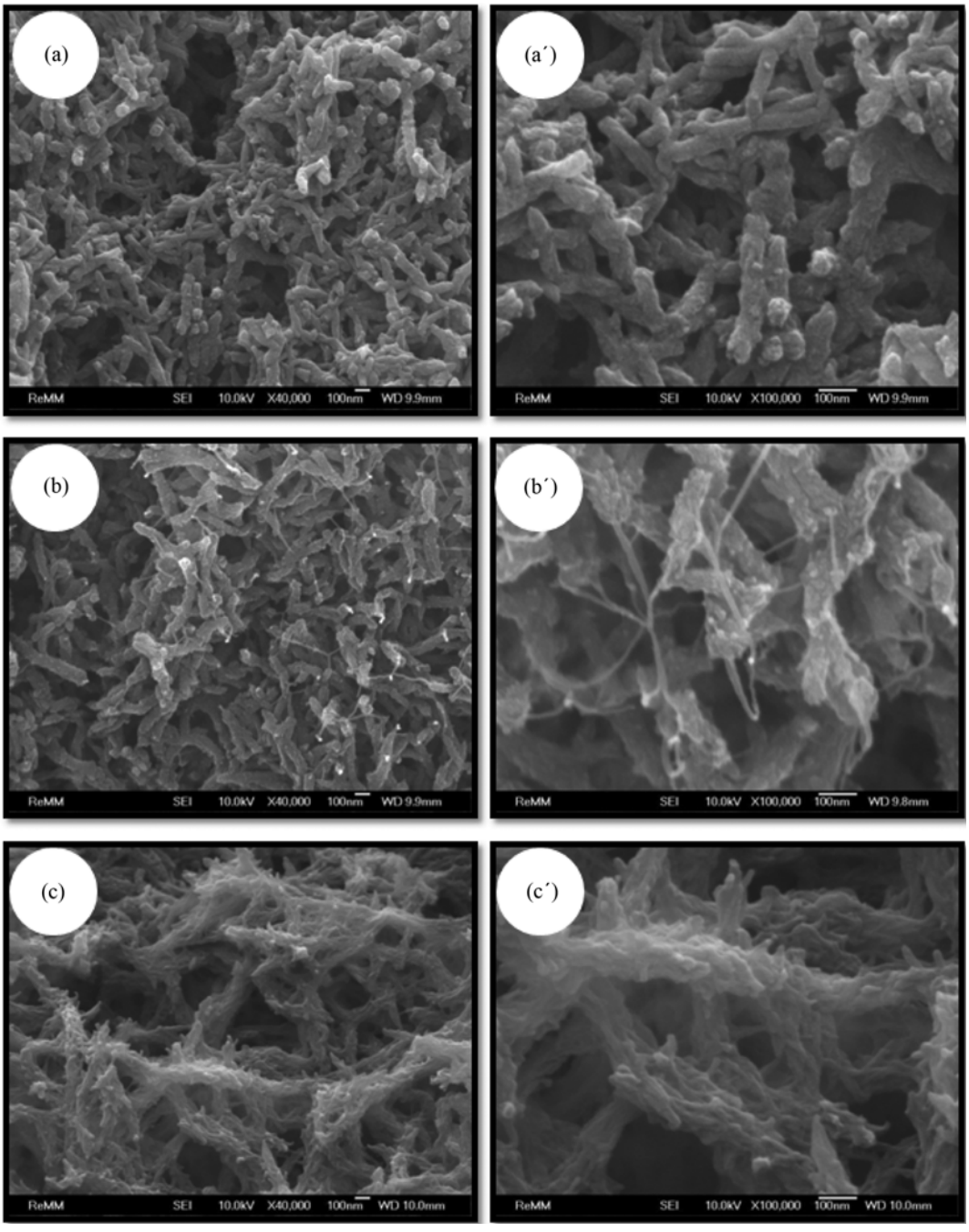

Fig. 4. SEM images of PANI nanofibers prepared by varying the molar ratio of aniline and cobalt chloride, i.e., (a), (a′) 6 : 1, (b), (b′) 1 : 1, and (c), (c′) 1 : 6.

PANI nanofibers were 20% lower than the EC of the ordinary PANI nanofibers, possibly due to thin fibrous structures on the surfaces of the HSA PANI nanofibers.

Figs. 5(a) and 5(b) show the TGA results of ordinary PANI nanofibers and the HSA PANI nanofibers, respectively. The analysis of ordinary PANI nanofibers was performed as a reference. As shown in Fig. 5(a), ordinary PANI nanofibers exhibited weight loss at low temperature range (<200 °C) mainly due to the loss of moisture on the surfaces. Additional weight loss was caused by the release of water and doping substances from the surfaces of the PANI nanofibers (200-470 °C) and the chemical decomposition of the polymers (470-800 °C) [52]. The TGA results of the HSA PANI nanofibers are shown in Fig. 5(b). The general weight loss across the whole temperature range was similar to that of ordinary PANI nanofibers. For ordinary PANI nanofibers, the maximum thermal decomposition in nitrogen occurred at 540 °C and the intensity of the peak was small. However, for the HSA PANI nanofibers, the temperature to show maximum weight loss shifted to a lower value, 484 °C, and the intensity of the peak greatly increased even though large-scale thermal decomposition of PANI occurred from 350 to

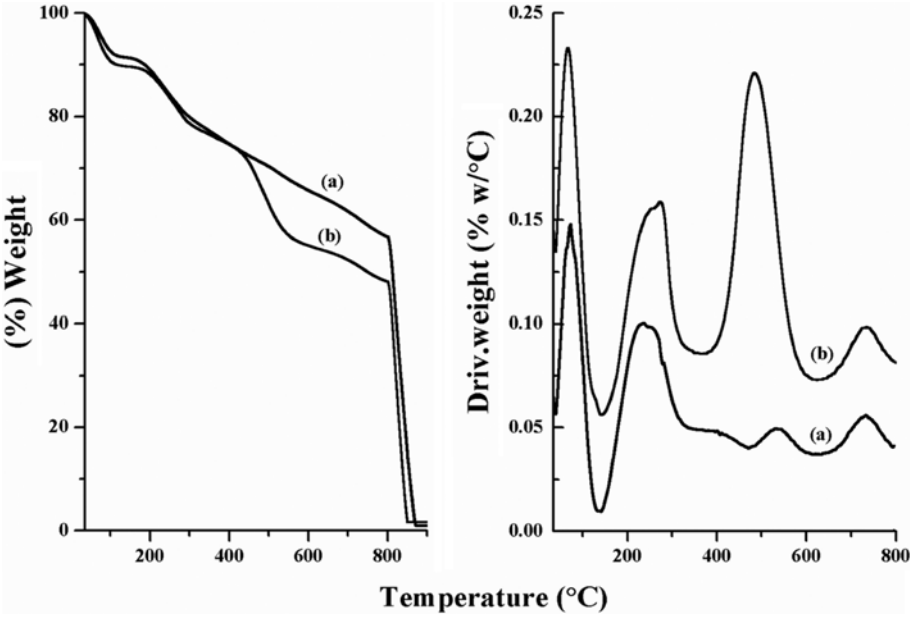

Fig. 5. TGA results of (a) ordinary PANI nanofibers and (b) HSA PANI nanofibers.

650 °C. The temperature shift as well as the intensity increase was attributed to the large amount of doping substances on the surfaces of the HSA PANI nanofibers.

The weight loss in the temperature range of 350-470 °C due to the release of doping substances from the surfaces of PANI [52] was 5.57% and 8.23% for ordinary and the HSA PANI nanofibers, respectively. These values revealed that the HSA PANI nanofibers contained more doping substances than did ordinary PANI nanofibers. Furthermore, the total weight loss percentage of ordinary PANI nanofibers and the HSA PANI nanofibers at 350-650 °C was 13.3% and 22.6%, respectively. Since the thermal degradation temperature of thin nanofibers was lower than that of thick nanofibers, the HSA PANI nanofibers that contained a large amount of thin nanofibers on the surface of the PANI backbone showed greater weight loss than did ordinary PANI nanofibers.

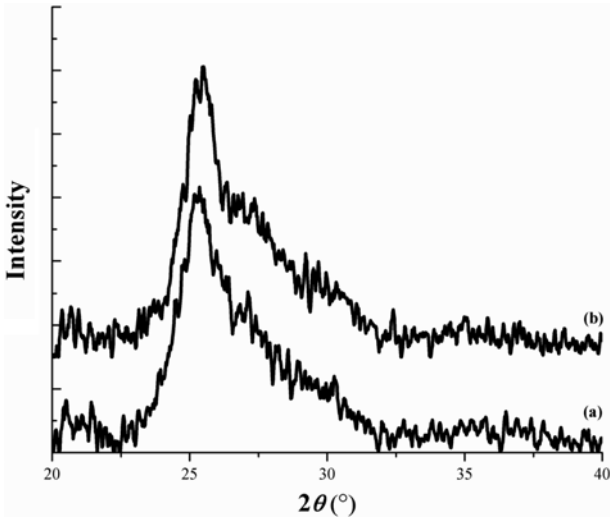

Fig. 6. XRD patterns of (a) ordinary PANI nanofibers and (b) HSA PANI nanofibers.

5. XRD Analysis of the PANI Nanofibers

The XRD pattern of the ordinary PANI nanofibers synthesized in compressed CO_2 has been reported previously [21]. Based on the XRD analysis of the ordinary PANI nanofibers in Fig. 6(a), it has been concluded that the PANI nanofibers were one-dimensional, branchless and crystalline. A single peak at 2θ=25° has been identified in the XRD pattern, which represented periodicity perpendicular to the polymer chain of PANI [21,53,54]. The XRD pattern of the HSA PANI nanofibers in Fig. 6(b) also shows that the HSA PANI nanofibers were crystalline with single Bragg diffraction peak at 2θ~25.52° (d~3.54 Å). If the PANI nanofibers had branches, the XRD pattern should have diffraction peak at 2θ=20° [54]. Since the XRD pattern of the HSA PANI in this work showed only one peak at 2θ~25.52°, it could be said that the HSA PANI nanofibers were branchless one-dimensional. Although the HSA PANI nanofibers had a coarse surface due to thin nanofibers on the surface of the nanofiber backbone, the HSA PANI nanofibers were composed of one-dimensional nanofibers without branches.

6. Performance as a Hydrogen Sensor

The performance as a hydrogen sensor was investigated by monitoring the resistance change in the HSA PANI nanofiber film upon exposure to hydrogen gas. The hydrogen sensor was tested at 25 °C with alternating cycles of exposure/removal of hydrogen gas (1% V/V). Among our experimental data, we showed only three cycles of response curve in Fig. 7 in order to examine the sensitivity of the sensor. The result showed that the sensor resistance varied alternately with and without the presence of hydrogen gas. In this work we used the highest grade hydrogen and nitrogen gases to minimize the water content since the resistance of PANI could be decreased in the presence of water vapor [33,55]. When the HSA PANI nanofiber film was exposed to hydrogen gas, the resistance increased rapidly, and subsequent exposure to air decreased the resistance of the sensor to the initial value. The resistance showed

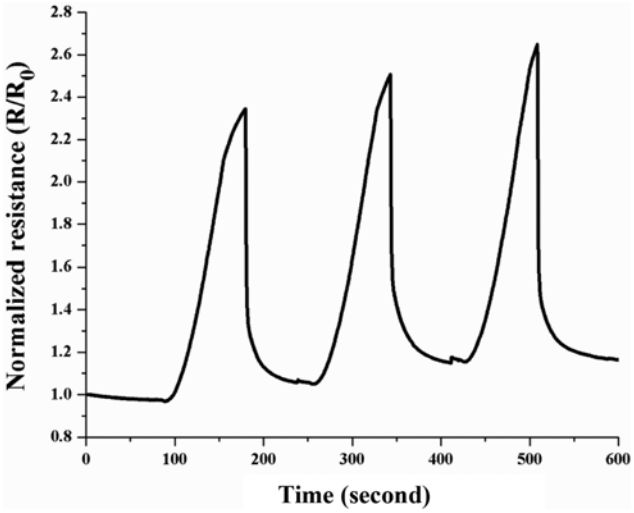

Fig. 7. Response of the hydrogen sensor composed of HSA PANI nanofiber film when exposed to 1% (V/V) hydrogen in nitrogen at 25 °C.

a 140% increase upon exposure to 1% hydrogen gas in N_2 such that the detection limit of this sensor could be much lower than 1%.

To quantify the performance of the sensor, several properties such as response time, recovery time, limit of detection (LOD), and limit of quantification (LOQ) were utilized. The response time is the time required to reach the saturation (maximum) value of resistance when the sensor is exposed to hydrogen gas. The recovery time is the time returning to the base resistance value upon removal of hydrogen. As shown in Fig. 7, the response time and recovery time were approximately 90 and 60 s, respectively. These values were lower than those of previous hydrogen sensors based on different kinds of PANI nanofibers [2,33]. The LOD and LOQ were determined from the signal noise level of the blank run, and were defined by the three and ten times of the signal noise level of the blank run, respectively [56]. Since the lowest concentration of H_2 in N_2 gas was 500 ppm according to the limitation of the experimental apparatus in this work, the repeated cycles of exposure/removal of 500 ppm (V/V) of H_2 in N_2 gas were performed at 25 °C as shown in Fig. 8. To compare the signals clearly, Fig. 8 shows only four cycles of response curve. Based on the noise level of the blank run and the signal peak of 500 ppm H_2 in N_2 gas, the LOD and LOQ were determined to be 40 ppm and 133 ppm (V/V) hydrogen, respectively.

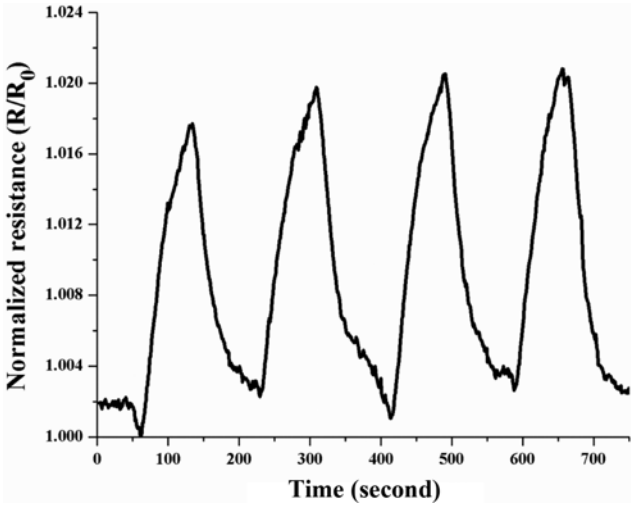

Fig. 8. Response of the hydrogen sensor composed of HSA PANI nanofiber film when exposed to 500 ppm (V/V) hydrogen in nitrogen at 25 °C.

To understand the behavior of a hydrogen sensor, a mechanism of increasing resistance is proposed. The conductivities of the HSA PANI nanofibers depend both on the oxidation state of the main polymer chain and the degree of protonation on the imine sites [57]. When the sensor is exposed to hydrogen, the penetrated hydrogen interacts with the HSA PANI nanofibers [32] and reacts with cobalt ions (or cobalt complex) to form cobalt hydride such that the transport of electrons to the surface of the HSA PANI nanofiber is decreased. Since the formation of a cobalt hydride deterred the electron transport into the nanofibers, the resistance of the HSA PANI nanofiber film increased upon exposure to hydrogen. At the recovery step, oxygen diffuses freely through the PANI nanofiber structures and reacts with cobalt hydride to form water and cobalt ions (or cobalt complex), which results in the returning of resistance to its original value. The transduction modes of hydrogen sensor based on PANI nanofibers showed different behaviors depending on the metal electrode employed [33,58] or thermal treatment of PANI [34]. Even though the mechanism of increasing resistance is proposed based on the formation of cobalt hydride, the effect of aluminum electrode needs to be evaluated in order to fully understand the behavior of the hydrogen sensor in this work. Therefore, investigations about the sensors using ordinary PANI/Al electrode or HSA PANI/Au electrode are necessary in the future communication.

The HSA PANI nanofibers exhibited excellent hydrogen sensing properties due to a high surface area and the presence of cobalt ions even though the amount was very small (0.46% from the EDS analysis). Since the high surface area of the HSA PANI nanofibers made it easy for hydrogen gases to diffuse into and out of the nanofiber film, the rapid response time could be possible. Moreover, the reactive sites of the HSA PANI nanofiber films composed of cobalt ions (or cobalt complexes) increased the sensitivities of the hydrogen sensor and showed much greater signals than those of conventional PANI films. In addition to the characteristics of PANI nanofibers in hydrogen gas sensors, the adhesion between spin-coated PANI nanofibers and silicon substrate greatly affects the performance of the hydrogen gas sensors [58]. Investigations about the adhesion are necessary in order to improve the efficiencies of the hydrogen gas sensors. Systematic studies on the reproducibility of the hydrogen sensors using HSA PANI and the performance of sensors relating to the adhesion deserve further detailed investigation.

CONCLUSIONS

HSA PANI nanofibers were synthesized successfully in compressed CO_2 using cobalt chloride as an additive. From SEM and TEM analyses, the HSA PANI nanofibers had coarse surfaces composed of very thin PANI nanofibers with 5-10 nm diameters. The HSA PANI

nanofibers had larger diameters than those of ordinary PANI nanofibers, such that the diameters of the HSA PANI nanofibers were within the range of 70-90 nm while those of ordinary PANI nanofibers were 30-70 nm. The electrical conductivity of the HSA PANI nanofibers was 3.46 S/cm, which is 20% lower than EC of the ordinary PANI nanofibers. Since the weight loss of the HSA PANI nanofibers was much greater than that of ordinary PANI nanofibers as observed from TGA analyses, it could be concluded that the HSA PANI nanofibers had more doping substances than did ordinary PANI nanofibers. The specific surface areas measured using BET method for ordinary and HSA PANI nanofibers were 37.9 and 68.4 m^2/g, respectively. The XRD results showed that the HSA PANI nanofibers had a crystalline structure as well as a branchless, one-dimensional form even though the coarse surface was covered by thin nanofibers. The HSA PANI nanofiber film was used to fabricate a hydrogen sensor showing large resistance increase upon exposure to hydrogen gas. The hydrogen sensor in this work possessed excellent characteristics to show high sensitivity and a short response time. And the LOD and LOQ of the hydrogen sensor resulted in very low values, which were 40 ppm and 133 ppm (V/V), respectively.

ACKNOWLEDGEMENTS

This work was supported by the 2015 Research Fund of University of Ulsan.

REFERENCES

1. J. Huang, S. Virji, B. H. Weiller and R. B. Kaner, *J. Am. Chem. Soc.*, **125**, 314 (2003).
2. R. Arsat, X. F. Yu, Y. X. Li, W. Wlodarski and K. Kalantar-Zadeh, *Sens. Actuat. B*, **137**, 529 (2009).
3. A. Z. Sadek, W. Wlodarski, K. Kalantar-Zadeh, C. Baker and R. B. Kaner, *Sens. Actuat. A*, **139**, 53 (2007).
4. H. Zhang, R. Liu and J. Zheng, *Synth. Met.*, **167**, 5 (2013).
5. G. D. Khuspe, S. T. Navale, M. A. Cougule and V. B. Patil, *Synth. Met.*, **185**, 1 (2013).
6. C. Murugan, E. Subramanian and D. P. Padiyan, *Synth. Met.*, **192**, 106 (2014).
7. P. A. Kumar, S. Chakraborty and M. Ray, *Chem. Eng. J.*, **141**, 130 (2008).
8. D. Mahanta, G. Madras, S. Radhakrishnan and S. Patil, *J. Phys. Chem. B*, **112**, 10153 (2008).
9. L. A. M. Ruotolo and J. C. Gubulin, *React. Funct. Polym.*, **62**, 141 (2005).
10. M. S. Lashkenari, B. Davodi and H. Eisazadeh, *Korean J. Chem. Eng.*, **28**, 1532 (2011).
11. S. S. Srinivasan, R. Ratnadurai, M. U. Niemann, A. R. Phani, D. Y. Goswami and E. K. Stefanakos, *Int. J. Hydrogen Energy*, **35**, 225 (2010).
12. S. Li, G. Zhang, G. Jing and J. Kan, *Synth. Met.*, **158**, 242 (2008).
13. J. Huang, S. Virji, B. H. Weiller and R. B. Kaner, *J. Am. Chem. Soc.*, **125**, 314 (2003).
14. X. B. Yan, Z. J. Han, Y. Yang and B. K. Tay, *Sens. Actuat. B*, **123**, 107 (2007).
15. H. Mi, X. Zhang, S. Yang, X. Ye and J. Luo, *Mater. Chem. Phys.*, **112**, 127 (2008).
16. H. Mi, X. Zhang, X. Ye and S. Yang, *J. Power Sources*, **176**, 403 (2008).
17. G. Ćirić-Marjanović, *Synth. Met.*, **177**, 1 (2013).
18. H. D. Tran, J. M. D'Arcy, Y. Wang, P. J. Beltramo, V. A. Strong and R. B. Kaner, *J. Mater. Chem.*, **21**, 3534 (2011).
19. J. Stejskal, I. Sapurina and M. Trchová, *Prog. Polym. Sci.*, **35**, 1420 (2010).
20. E. C. Venancio, P.-C. Wang and A. G. MacDiarmid, *Synth. Met.*, **156**, 357 (2006).
21. Q. M. Pham, J.-S. Kim and S. Kim, *Synth. Met.*, **160**, 394 (2010).
22. Z. Zhang, Z. Wei, L. Zhang and M. Wan, *Acta Mater.*, **53**, 1373 (2005).
23. G. Li, S. Pang, G. Xie, Z. Wang, H. Peng and Z. Zhang, *Polymer*, **47**, 1456 (2006).
24. Y. Guo and Y. Zhou, *Eur. Polym. J.*, **43**, 2292 (2007).
25. T. Thanpitcha, A. Sirivat, A. M. Jamieson and R. Rujiravanit, *Eur. Polym. J.*, **44**, 3423 (2008).
26. Z. Zhang, J. Deng, L. Yu and M. Wan, *Synth. Met.*, **158**, 712 (2008).
27. B. Panella, L. Kossykh, U. Dettlaff-Weglikowska, M. Hirscher, G. Zerbi and S. Roth, *Synth. Met.*, **151**, 208 (2005).
28. M. U. Jurczyk, A. Kumar, S. Srinivasan and E. Stefanakos, *Int. J. Hydrogen Energy*, **32**, 1010 (2007).
29. S. J. Cho, K. Choo, D. P. Kim and J. W. Kim, *Catal. Today*, **120**, 336 (2007).
30. J. Germain, J. M. J. Fréchet and F. Svec, *J. Mater. Chem.*, **17**, 4989 (2007).
31. A. Rahy, T. Rguig, S. J. Cho, C. E. Bunker and D. J. Yang, *Synth. Met.*, **161**, 280 (2011).
32. S. Virji, R. B. Kaner and B. H. Weiller, *J. Phys. Chem. B*, **110**, 22266 (2006).
33. J. D. Fowler, S. Virji, R. B. Kaner and B. H. Weiller, *J. Phys. Chem. C*, **113**, 6444 (2009).
34. P.-C. Wang, Y. Dan and L.-H. Liu, *Mater. Chem. Phys.*, **144**, 155 (2014).
35. J. L. Kendall, D. A. Canelas, J. L. Young and J. M. DeSimone, *Chem. Rev.*, **99**, 543 (1999).
36. A. I. Cooper, *J. Mater. Chem.*, **10**, 207 (2000).
37. E. J. Beckman, *J. Supercrit. Fluids*, **28**, 121 (2004).
38. S. P. Nalawade, F. Picchioni and L. P. B. M. Janssen, *Prog. Polym. Sci.*, **31**, 19 (2006).
39. M. Y. Kim, K.-P. Yoo and J. S. Lim, *Korean J. Chem. Eng.*, **24**, 860 (2007).
40. J. G. Masters, Y. Sun, A. G. MacDiarmid and A. J. Epstein, *Synth. Met.*, **41**, 711 (1991).
41. P.-C. Wang, Z. Huang and A. G. MacDiarmid, *Synth. Met.*, **101**, 852 (1999).
42. P.-C. Wang, E. C. Venancio, D. M. Sarno and A. G. MacDiarmid, *React. Funct. Polym.*, **69**, 217 (2009).
43. X. Jing, Y. Wang, D. Wu and J. Qiang, *Ultrason. Sonochem.*, **14**, 75 (2007).
44. N.-R. Chiou and A. J. Epstein, *Synth. Met.*, **153**, 69 (2005).
45. A. Rahy, M. Sakrout, S. Manohar, S. J. Cho, J. Ferraris and D. J. Yang, *Chem. Mater.*, **20**, 4808 (2008).
46. H. D. Tran, Y. Wang, J. M. D'Arcy and R. B. Kaner, *ACS Nano*, **2**, 1841 (2008).

47. Y. Wang and X. Jing, *J. Phys. Chem. B*, **112**, 1157 (2008).
48. X. Zhang, R. Chan-Yu-King, A. Jose and S. K. Manohar, *Synth. Met.*, **145**, 23 (2004).
49. N.-R. Chiou and A. J. Epstein, *Adv. Mater.*, **17**, 1679 (2005).
50. K. Gupta, G. Chakraborty, S. Ghatak, P. C. Jana and A. K. Meikap, *J. Appl. Polym. Sci.*, **115**, 2911 (2010).
51. D. Zhang, *Polym. Test.*, **26**, 9 (2007).
52. S. Bhadra and D. Khastgir, *Polym. Degrad. Stab.*, **92**, 1824 (2007).
53. S. Bhadra and D. Khastgir, *Polym. Test.*, **27**, 851 (2008).
54. L. Zhang and M. Wan, *Adv. Funct. Mater.*, **13**, 815 (2003).
55. M. Angelopoulos, A. Ray and A. G. MacDiarmid, *Synth. Met.*, **21**, 21 (1987).
56. D. A. Armbruster and T. Pry, *Clin. Biochem. Rev.*, **29 Suppl 1**, S49 (2008).
57. A. G. MacDiarmid, *Synth. Met.*, **125**, 11 (2001).
58. D. Nicolas-Debarnot and F. Poncin-Epaillard, *Anal. Chim. Acta*, **475**, 1 (2003).